LETTER

doi:10.1038/nature23901

Patchy particles made by colloidal fusion

Zhe Gong[1], Theodore Hueckel[1], Gi-Ra Yi[2] & Stefano Sacanna[1]

Patches on the surfaces of colloidal particles[1–5] provide directional information that enables the self-assembly of the particles into higher-order structures. Although computational tools can make quantitative predictions and can generate design rules that link the patch motif of a particle to its internal microstructure and to the emergent properties of the self-assembled materials[6–8], the experimental realization of model systems of particles with surface patches (or 'patchy' particles) remains a challenge. Synthetic patchy colloidal particles are often poor geometric approximations of the digital building blocks used in simulations[9,10] and can only rarely be manufactured in sufficiently high yields to be routinely used as experimental model systems[11–14]. Here we introduce a method, which we refer to as colloidal fusion, for fabricating functional patchy particles in a tunable and scalable manner. Using coordination dynamics and wetting forces, we engineer hybrid liquid–solid clusters that evolve into particles with a range of patchy surface morphologies on addition of a plasticizer. We are able to predict and control the evolutionary pathway by considering surface-energy minimization, leading to two main branches of product: first, spherical particles with liquid surface patches, capable of forming curable bonds with neighbouring particles to assemble robust supracolloidal structures; and second, particles with a faceted liquid compartment, which can be cured and purified to yield colloidal polyhedra. These findings outline a scalable strategy for the synthesis of patchy particles, first by designing their surface patterns by computer simulation, and then by recreating them in the laboratory with high fidelity.

Unlike regular spherical colloids such as silica or polystyrene beads, patchy particles carry a considerable amount of self-assembly information. For example, their coordination number, bond angles and selectivity are all programmable by rationally designing the number and topological distribution of patches and their chemical composition. The intuitively simple idea of patchy particles, however, comes with the challenge of creating such surface patterns in a controllable, reproducible and scalable manner. Colloidal fusion addresses this challenge with a new approach to the synthesis of patchy particles based on the concept of surface evolution—the morphological transformation of an object under the combined effects of surface tension and geometrical constraints. We introduce colloidal fusion in Fig. 1a with the help of a macroscopic model system analogue. Let us consider a regular tetrahedral cluster of four malleable spheres arranged around a smaller and softer core. When spherical pressure is applied to the tetrahedral cluster it deforms, and as it gradually morphs into a spherical object its core extrudes through the interstices to form four precisely coordinated patches. In contrast to classic synthetic methodologies, colloidal fusion does not rely heavily on chemistry. Instead, it builds on a simple physicochemical algorithm, in which the symmetry and composition of the cluster are added to a system as information, after which the system is compiled by applying pressure to obtain the target patchy particle. Applying this algorithm to a colloidal system requires two essential ingredients: malleable hybrid clusters, and a suitable driving force to actuate the deformation. Following the example of Fig. 1a, we first describe the synthesis of patchy particles with a tetrahedral motif, and then generalize the method for increasingly complex patchy patterns.

Regular colloidal clusters are traditionally formed by allowing random numbers of spheres N to pack inside drying emulsion droplets and then sorting the clusters by size[15]. In contrast, tetrahedral clusters may be logically assembled from bi-dispersed suspensions via controlled heteroaggregation, whereby four shell particles bind irreversibly to an oppositely charged core[16]. Experiments and computer simulations have shown that when the ratio α of shell to core radius approaches 2.41, the stochastic aggregation process results in a nearly quantitative (nearly 100%) yield of tetrahedral clusters. However, at this size ratio, the clusters are loosely packed and only poorly approximate regular tetrahedra. Achieving symmetric clusters via heteroaggregation requires reconfiguration and, although tunable soft interactions may allow for this, dense packing can be naturally achieved by using a liquid core. A liquid core introduces another phenomenon that occurs in parallel to the random coordination, whereby the core wets the shell particles. With proper control, wetting effectively pulls shell particles together, resulting in high yields of liquid-core colloidal clusters (LCCs) with regular tetrahedral symmetry. We assemble LCCs by mixing silicone-based emulsion droplets[17] with a dense suspension of polystyrene spheres (Extended Data Fig. 1). The correct assembly of a tetrahedral LCC depends crucially on two concerted events: the rapid coordination of four shell particles around a liquid droplet, and their slow sinkage in the oil due to wetting. The rapid coordination dynamics is necessary to allow all four shell particles to park onto the surface of the droplet before any substantial wetting occurs, which would otherwise change the effective value of α and lower the yield of tetrahedral clusters. After the shell is fully assembled, the slower wetting dynamics allows the cluster to gradually compact and rearrange into a symmetric LCC (Extended Data Fig. 2a).

Because this process is intrinsically controlled by geometrical constraints, it is particularly robust; as long as the value of α is kept constant, tetrahedral LCCs reliably self-assemble from building blocks of various sizes and chemical compositions. This enables the production of nanometre- and micrometre-scale LCCs, and permits the impartation of specific chemical functionalities to core and shell materials independently. Figure 1b illustrates the assembly of LCCs from positively charged polystyrene spheres and methacrylate-functionalized silicone oil droplets. These particular materials allow for the hardening of liquid cores via radical polymerization, to create a robust product that can withstand drying (Fig. 1c). Solidified cores are also resistant to organic solvents, thus enabling the selective dissolution of the polystyrene spheres and direct visualization of the morphology of the cores via scanning electron microscopy (SEM)[18] (Fig. 1d).

The coordination of LCCs requires a large excess of shell particles to mitigate bridging between liquid cores. We found that a shell-to-core ratio of 100:1 is sufficient to obtain a nearly quantitative yield of tetrahedral clusters ($\geq$90%). After the assembly of LCCs, the density of the water phase is raised with glycerol such that low-density uncoordinated polystyrene shells rise to the top, while the clusters, with their denser cores, sediment to the bottom of the container (Fig. 1e–h).

[1]Molecular Design Institute, Department of Chemistry, New York University, 29 Washington Place, New York, New York 10003, USA. [2]School of Chemical Engineering, Sungkyunkwan University (SKKU), Suwon 16419, South Korea.

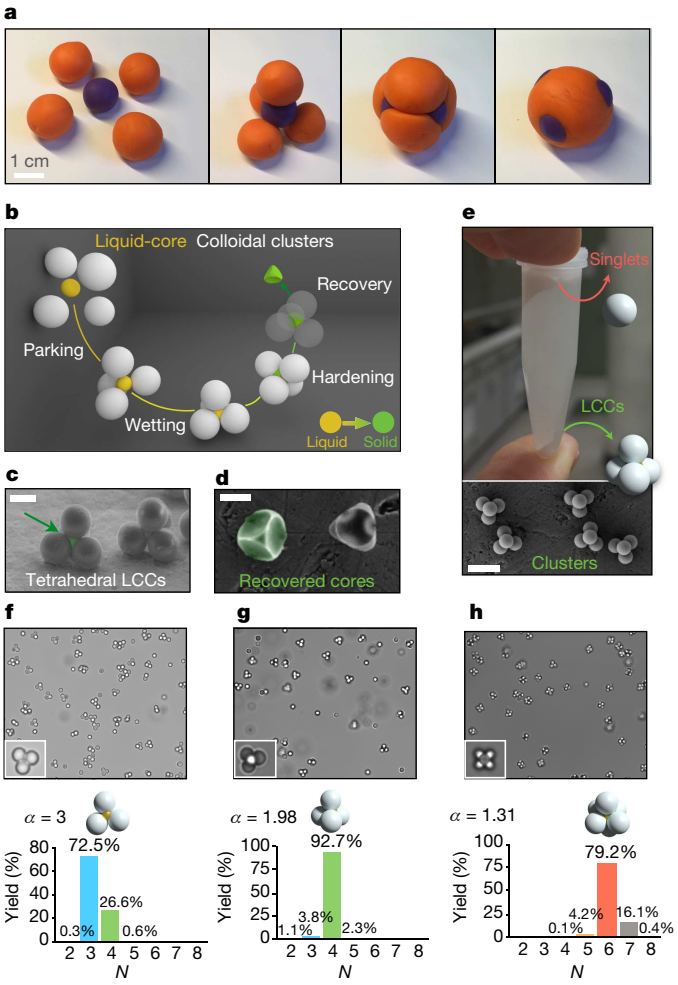

Figure 1 | Liquid-core colloidal clusters. a, Play-dough model illustrating the concept of colloidal fusion. When spherically compressed, the symmetry and composition of the cluster determine its evolutionary path and the patchy motif of the resulting sphere. **b**, Schematics showing the assembly of a liquid-core colloidal cluster (LCC). The wetting of the solid shells enables reconfiguration, and thus close-packing. The liquid core can be chemically hardened and then recovered by dissolving the shell particles. **c**, **d**, SEM images showing polymerized hybrid tetrahedral clusters (**c**) and polystyrene imprinted solid cores (**d**). **e**, Owing to their different effective densities, LCCs and single polystyrene spheres (singlets) can be efficiently separated via a single centrifugation step in a medium with intermediate density. The picture (upper panel) shows LCCs sedimented at the bottom of a centrifuge tube that contains a water/glycerol mixture and singlets at the top. The SEM image (lower panel) shows the purified clusters. Scale bars in **c**–**e** are 1 μm. **f**–**h**, Bright-field optical microscopy images (upper panels) showing unpurified samples of LCCs assembled at $\alpha = 3$ (**f**), $\alpha = 1.98$ (**g**) and $\alpha = 1.31$ (**h**), with insets showing the major species. Statistical distributions of the coordination number N for clusters that form at various a are shown in the bottom panels.

The unreacted polystyrene shells are then recycled, whereas the LCCs are isolated for further processing. Because glycerol splitting depends only on the density contrast between core and shell materials, the same glycerol concentration may be used to split LCCs of any size. In our experiments, we successfully isolated clusters ranging in size from 400 nm to 4 μm (Extended Data Fig. 2b, c).

Because of their large overall surface, LCCs can be thought of as high-energy intermediates that spontaneously evolve into spherical objects when opportunely plasticized. Such evolution is driven by surface-energy minimization, and is experimentally actuated by adding a small amount of tetrahydrofuran to the colloidal suspension. Similarly to what was previously reported for the synthesis of other anisotropic polymer colloids via liquid intermediates, tetrahydrofuran (THF) acts as a plasticizer allowing the polystyrene spheres to flow under the action of surface tension[3,18–20]. The time-lapse in Fig. 2a illustrates the evolution of a tetrahedral LCC with a fluorescently labelled core. As the contours of the cluster gradually morph into a sphere, fluorescence microscopy reveals that the core material is squeezed through the interstices of the cluster and reaches the surface of the particle where it forms four tetrahedrally coordinated liquid patches (see also Supplementary Video 1). This extrusion process provides a transcription mechanism that converts the symmetry of the cluster into a well-defined patch design, and is the key to the formation of the liquid patches. For a correct transcription, however, two main conditions have to be met.

First, colloidal fusion should not permit intermixing between the constituent building blocks of the LCCs. In the LCC described above, for example, the four polystyrene particles that form the cluster should not coalesce even when plasticized and, at the same time, they should not be miscible with the silicone oil core. Compartmentalization is necessary to preserve the structural integrity of the interstitial channels through which the core is extruded and to retain chemical contrast between the patches and matrix in the final product. This is illustrated in Fig. 2b, where we consider a mono-substituted LCC that features a fluorescently labelled shell particle. As expected, colloidal fusion causes the cluster to deform into a sphere; however, the fluorescent signal does not spread homogeneously to the entire particle, but instead remains well confined within a single quadrant, thus confirming the cellular structure of the resulting patchy particle. Experimentally, we prevent coalescence by using surfactants (such as polyvinylpyrrolidone (PVP)-stabilized polystyrene spheres and Pluronic-F108-coated emulsion droplets) and charged interfaces (such as oil droplets with negatively charged surface groups). By polymerizing the liquid core during the fusion process, we can capture the mechanics of the deformation in great detail. In fact, the polymerization enables us to fix a crucial intermediate state, in which the core material has not yet fully reached the surface of the particle but is still moving through the interstitial channels of the cluster. By dissolving the polystyrene matrix, this partially extruded core can be isolated and imaged using SEM to reveal an accurate replica of the interstitial channels of the cluster through which the extrusion has taken place (Fig. 2b).

The second condition for the successful evolution of an LCC into a patchy particle depends on the surface chemistry of the cluster. Because colloidal fusion is driven by surface-energy minimization, the fate of the LCC is determined by the interfacial tension γ between its constituent materials. In the systems described above, these values correspond to $\gamma_{PSl/w}$, $\gamma_{o/w}$ and $\gamma_{PSl/o}$, where 'w' indicates the aqueous plasticizing solution (20%–40% THF), 'PSl' is plasticized polystyrene and 'o' is silicone oil. The interplay between these forces determines the propensity of the LCC to evolve into a patchy particle or to retain the more familiar core–shell structure. Because γ is affected by pH, surfactants and temperature, this propensity may be enhanced or diminished by changing the experimental conditions. For example, in Fig. 2c we show that when a LCC undergoes colloidal fusion at pH 7, its core erupts to the surface of the particle to form a liquid patch; however, at pH 2 we observe empty holes corresponding to the interstitial channels, indicating that the liquid core prefers to remain fully engulfed inside the particle at the new experimental conditions. As we show in Extended Data Fig. 3, the pH changes the surface charge density of the components of the cluster, causing a corresponding change in the wetting angle between oil and polystyrene, and ultimately a different deformation behaviour.

Although the experimental conditions for successful colloidal fusion can be found via relatively simple iterative trial and error processes, computer simulations offer more elegant and effective approaches to assist the design process. Surface Evolver[21,22], in particular, can be used as a predictive tool to anticipate the evolutionary pathway of an LCC as a function of its symmetry and material composition. As we show in

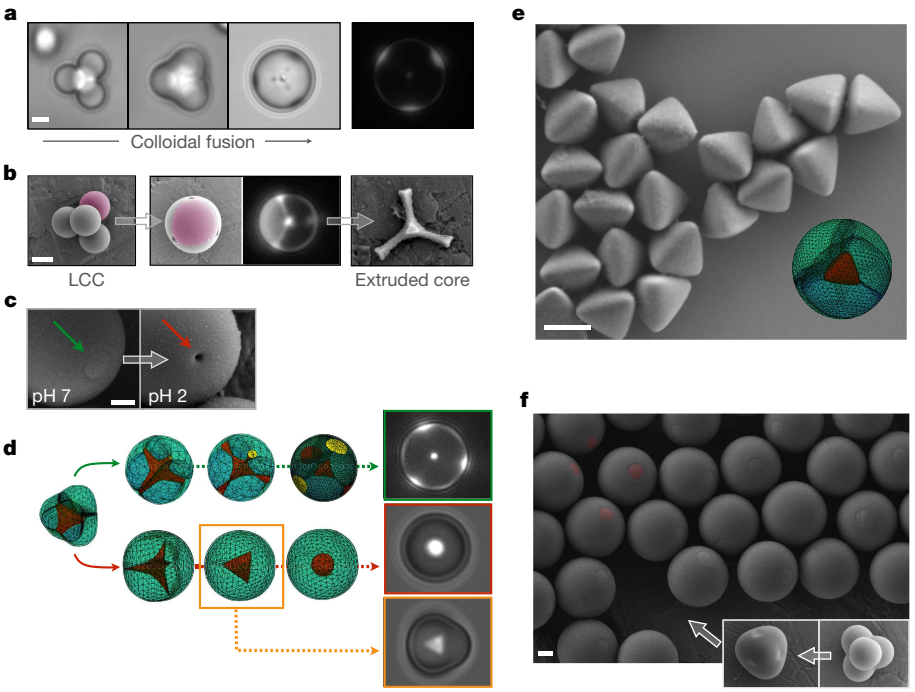

Figure 2 | Colloidal fusion. a, Bright-field time-lapse images (left) and a fluorescence microscopy image at the final time point (right) showing the deformation of a tetrahedral LCC after the addition of a plasticizer. The plasticized shell particles fuse together and the fluorescent liquid core is squeezed through the interstices of the cluster to form surface patches. **b**, False-colour SEM images showing a mono-substituted tetrahedral LCC carrying one fluorescently labelled shell particle (pink). Upon deformation, the fluorescent signal remains confined in a single quadrant of the resulting patchy particle, confirming the compartmentalization and the absence of coalescence events between the original shell particles. On the right, SEM captures the morphology of the extruded core. **c**, Under good wetting conditions (pH 7) the liquid core extrudes through the interstices of the cluster forming visible liquid patches on the surface of the particle (green arrow). Under poor wetting conditions (pH 2), however, the core remains buried inside the particle, leaving empty interstitial channels (red arrow). **d**, Surface Evolver simulations showing two different fusion paths. Depending on the relative surface energies of the components of the LCC, colloidal fusion can lead to a patchy (green path) or a core–shell (red path) morphology (Extended Data Fig. 5). Intermediate states display anisotropic inner microstructures that include faceted cores (orange) (Extended Data Fig. 4). On the right, fluorescent microscopy images show the corresponding experimental morphologies obtained by evolving LCCs at different values of pH (and so with different surface energies). **e**, Intermediate core morphologies can be fixed by polymerization and then recovered by dissolving the encasing polystyrene matrix. The SEM image shows faceted colloidal tetrahedra resulting from polymerization; recovery of the intermediate microstructure is highlighted in the inset. **f**, SEM image of polymerized patchy particles (some patches are false-coloured). The insets show SEM images of deformed clusters with increasing degrees of plasticization. All scale bars are 1 μm.

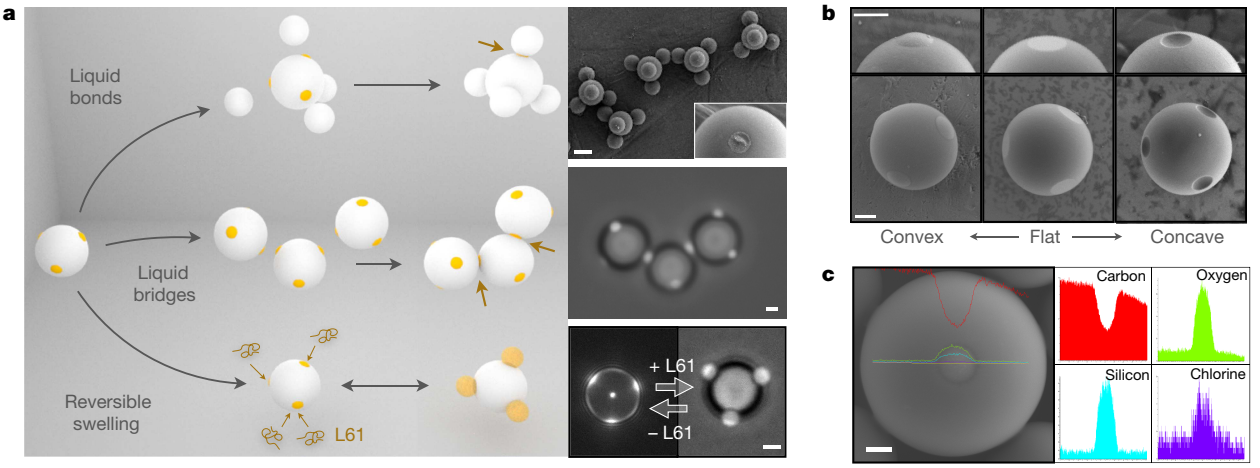

Figure 3 | Liquid patches. a, Liquid patches enable unique self-assembly capabilities. In this scheme, for example, we illustrate how patchy particles can form liquid bonds with target particles or patch-to-patch liquid bridges with each other (brown arrows). The resulting assemblies can be fixed by a polymerization reaction and examined using SEM. Moreover, in their liquid state, the patches can be selectively and reversibly swollen by organic molecules, thus introducing the ability to dynamically change their local morphology. On the right, experimental data showing (from top to bottom): (i) supracolloidal clusters assembled via liquid bonding and fixed by radical polymerization (the inset shows the details of a (broken) bond); (ii) fluorescent microscopy image showing patchy particles interconnected by liquid bridges; and (iii) fluorescent microscopy image showing a patchy particle before and after patch-swelling by Pluronic L61. **b**, The liquid nature of the patches enables us to change their curvature by gradually dissolving the oil phase or altering its wetting angle. The figure shows SEM images of patchy particles with different patch curvature. **c**, Energy-dispersive X-ray spectroscopy of a patchy particle made of chlorinated silicone oil and PVP–polystyrene. The spectra on the right indicate the relative abundance of carbon, oxygen, silicon and chlorine along the scanned line (yellow line in the left panel). All scale bars are 1 μm.

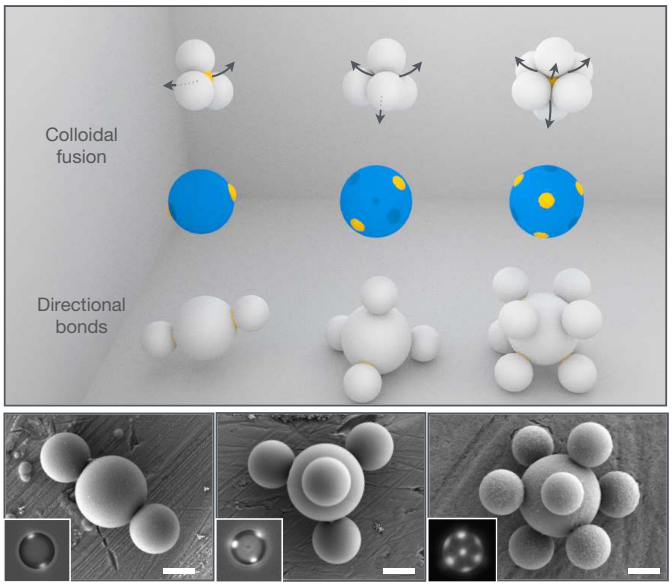

Figure 4 | Predictable patchy motifs. Schematics of liquid-core extrusion and directional bonds of three types of LCC. SEM image at the bottom show coordinated patchy particles with particles directionally sticking to patches. Insets are optical images of corresponding patchy particles with fluorescent patches. All scale bars are 1 μm.

Fig. 2d, Surface Evolver simulations accurately capture the dynamics of core extrusion and patch formation, and also predict, for increasing $\gamma_{PSl/o}$, an alternative path that leads to a core–shell structure. Specific internal microstructures along these deformation paths can be targeted as sources of new colloidal geometries. For example, the red path shown in Fig. 2d reveals the existence of an intermediate microstructure in which the liquid core displays a faceted tetrahedral shape (Extended Data Fig. 4). Experimentally, this microstructure has been detected by fluorescence microscopy, fixed by polymerization and recovered by dissolving the encasing polystyrene matrix (Fig. 2e). Similarly, patchy particles resulting from evolution via the green path are shown in Fig. 2f.

In a typical Surface Evolver simulation we fix $\gamma_{PSl/w}$, $\gamma_{o/w}$ and the oil-to-polystyrene volume ratio on the basis of the experimental values and let the LCC evolve for different values of $\gamma_{PSl/o}$ (Extended Data Fig. 5; see also Extended Data Fig. 6). During the final step of the colloidal fusion process, the plasticizer is evaporated to harden the polystyrene body of the particle and permanently fix the patchy morphology. The patches on the body of the polystyrene spheres can also be hardened via radical polymerization. Notably, it is the liquid nature of the patches that gives the particles their unique capabilities. For example, in Fig. 3a we demonstrate that liquid bridges can create precise colloidal bonds to connect target colloids to patchy particles and enable patch-to-patch assemblies (Extended Data Fig. 7). Liquid bonds can be permanently fixed by polymerizing the oil phase, thus yielding robust supracolloidal architectures that can withstand drying forces.

Another distinctive feature of liquid patches is their ability to reversibly expand when exposed to a swelling agent. This is also demonstrated in Extended Data Fig. 8, in which a non-ionic triblock copolymer with low water solubility (Pluronic L61) is shown to selectively swell the liquid patches on the particle to several times their original volume.

More subtle changes to the morphology of the patches can be introduced by shrinking the liquid patch after colloidal fusion, which enables the fabrication of particles with convex, flat or concave patches (Fig. 3b). In our experiments, we successfully tested colloidal fusion on LCCs with three different types of core chemistry. Specifically, liquid cores consisting of 3-(trimethoxysilyl)propyl methacrylate, (3-chloropropyl) trimethoxy silane and (3-glycidyloxypropyl) trimethoxy silane were used to obtain methacryl-, chloro- and epoxy-substituted patches, respectively (Fig. 3c).

As we show in Fig. 4, colloidal fusion is not limited to tetrahedral clusters. By varying α, lower- and higher-order LCCs can be similarly assembled and then transformed into patchy particles with predictable patterns. In our experiments, we assembled LCCs with $N=3$ (trimers) and $N=6$ (hexamers) by varying α from 2.41 to 3.85 and to 1.5, respectively. We then evolved these two types of LCC into patchy particles (two- and eight-patch motif, respectively) following the same procedure described for tetrahedral clusters. Whereas tetrahedral LCCs form with yields above 90%, the yield of trimers and hexamers decreases below 80% because small amounts of higher- and lower-order clusters form concurrently[16], thus requiring an intermediate purification step.

Taken together, this work introduces a conceptually new form of scalable colloidal synthesis in which the use of geometric constraints and interfacial forces largely replace chemistry. In particular, uniform patchy particles with tetrahedral symmetry are quantitatively prepared via the controlled plasticization of composite clusters and then collected in single-step isopycnic centrifugation. Because the patches are chemically and physically distinct, they have many assembly capabilities. Looking forward, we envision manufacturing materials with unprecedented microstructural complexity by evolving—through colloidal fusion—higher-order clusters, binary colloidal crystals and other more elaborate composite architectures.

Online Content Methods, along with any additional Extended Data display items and Source Data, are available in the online version of the paper; references unique to these sections appear only in the online paper.

Received 27 March; accepted 2 August 2017.
Published online 18 September 2017.

1. Zhang, Z. & Glotzer, S. Self-assembly of patchy particles. *Nano Lett.* **4,** 1407–1413 (2004).
2. Duguet, E., Hubert, C., Chomette, C., Perro, A. & Ravaine, S. Patchy colloidal particles for programmed self-assembly. *C. R. Chim.* **19,** 173–182 (2016).
3. Wang, Y. *et al.* Colloids with valence and specific directional bonding. *Nature* **491,** 51–55 (2012).
4. Pawar, A. B. & Kretzschmar, I. Fabrication, assembly, and application of patchy particles. *Macromol. Rapid Commun.* **31,** 150–168 (2010).
5. Hubert, C. *et al.* Synthesis of multivalent silica nanoparticles combining both enthalpic and entropic patchiness. *Faraday Discuss.* **181,** 139–146 (2015).
6. van Anders, G., Klotsa, D., Karas, A. S., Dodd, P. M. & Glotzer, S. C. Digital alchemy for materials design: colloids and beyond. *ACS Nano* **9,** 9542–9553 (2015).
7. Bianchi, E., Largo, J., Tartaglia, P., Zaccarelli, E. & Sciortino, F. Phase diagram of patchy colloids: towards empty liquids. *Phys. Rev. Lett.* **97,** 168301 (2006).
8. van Anders, G., Ahmed, N. K., Smith, R., Engel, M. & Glotzer, S. C. Entropically patchy particles: engineering valence through shape entropy. *ACS Nano* **8,** 931–940 (2014).
9. Romano, F. & Sciortino, F. Patterning symmetry in the rational design of colloidal crystals. *Nat. Commun.* **3,** 975 (2012).
10. Smallenburg, F. & Sciortino, F. Liquids more stable than crystals in particles with limited valence and flexible bonds. *Nat. Phys.* **9,** 554–558 (2013).
11. Wang, Y. *et al.* Three-dimensional lock and key colloids. *J. Am. Chem. Soc.* **136,** 6866–6869 (2014).
12. Pawar, A. B. & Kretzschmar, I. Patchy particles by glancing angle deposition. *Langmuir* **24,** 355–358 (2008).
13. Chen, Q., Bae, S. C. & Granick, S. Directed self-assembly of a colloidal kagome lattice. *Nature* **469,** 381–384 (2011).
14. Jiang, S. & Granick, S. A simple method to produce trivalent colloidal particles. *Langmuir* **25,** 8915–8918 (2009).
15. Manoharan, V., Elsesser, M. & Pine, D. Dense packing and symmetry in small clusters of microspheres. *Science* **301,** 483–487 (2003).
16. Schade, N. B. *et al.* Tetrahedral colloidal clusters from random parking of bidisperse spheres. *Phys. Rev. Lett.* **110,** 148303 (2013).
17. Obey, T. & Vincent, B. Novel monodisperse "silicone oil"/water emulsions. *J. Colloid Interface Sci.* **163,** 454–463 (1994).
18. Sacanna, S. *et al.* Shaping colloids for self-assembly. *Nat. Commun.* **4,** 1688 (2013).
19. Kraft, D. J., Groenewold, J. & Kegel, W. K. Colloidal molecules with well-controlled bond angles. *Soft Matter* **5,** 3823–3826 (2009).
20. Kraft, D. J. *et al.* Self-assembly of colloids with liquid protrusions. *J. Am. Chem. Soc.* **131,** 1182–1186 (2009).
21. Brakke, K. A. The Surface Evolver. *Exp. Math.* **1,** 141–165 (1992).
22. Berthier, J & Brakke, K. A. *The Physics of Microdroplets* (Wiley, 2012).

Supplementary Information is available in the online version of the paper.

Acknowledgements This work was supported by the NSF CAREER award DMR-1653465. The Zeiss Merlin FESEM was acquired through the support of the NSF under award number DMR-0923251. G.-R.Y. acknowledges support from the NRF (Korea) under award numbers 2010-0029409 and 2014S1A2A2028608. We thank S. Phua for comments on the manuscript and discussions.

Author Contributions Z.G. and T.H. synthesized all of the colloidal systems, designed and performed the colloidal fusion experiments and analysed data; G.-R.Y. performed Surface Evolver simulations; S.S. conceived the study and supervised the research with the help of G.-R.Y.; S.S., G.-R.Y., Z.G. and T.H. wrote the manuscript. All authors discussed the results and commented on the manuscript.

Author Information Reprints and permissions information is available at www.nature.com/reprints. The authors declare no competing financial interests. Readers are welcome to comment on the online version of the paper. Publisher's note: Springer Nature remains neutral with regard to jurisdictional claims in published maps and institutional affiliations. Correspondence and requests for materials should be addressed to S.S. (s.sacanna@nyu.edu).

Reviewer Information *Nature* thanks N. Kotov, N. Vogel and the other anonymous reviewer(s) for their contribution to the peer review of this work.

METHODS

Synthesis of LCCs. LCCs are assembled from solid polystyrene (PS) spheres and silicone-based emulsion droplets via a simple heteroaggregation process. The assembly is driven either by electrostatic forces between oppositely charged species or by polymer bridging flocculation between PVP-coated PS spheres and oil droplets.

Liquid cores. Monodispersed emulsions are prepared by the hydrolysis and condensation reaction of three different functional silanes: 3-(trimethoxysilyl) propyl methacrylate (≥98% from Sigma-Aldrich), (3-chloropropyl) trimethoxy silane (≥97%, Sigma-Aldrich) and (3-glycidyloxypropyl) trimethoxy silane (≥98%, Sigma-Aldrich) (Extended Data Fig. 1a–d). These oil precursors are used pure or intermixed, depending on the chemical functionalities desired in the final product. Methacrylate functionalized droplets, for example, are prepared by adding 40 μl of NH_3 (28 wt%) to 160 ml deionized water, followed by the addition of 300 μl of 3-(trimethoxysilyl)propyl methacrylate. This mixture is kept under mild magnetic stirring for 1 h to allow the oil droplets to nucleate and grow to a final size of approximately 800 nm. By changing the ratio of ammonia and oil precursor we are able to tune the size of the droplets from 400 nm to more than 1 μm. Occasionally, the emulsions were fluorescently labelled using rhodamine-B isothiocyanate to allow for fluorescence microscopy. The coupling agent 3-aminopropyl trimethoxysilane was used to ensure covalent bonding between the dye and the oil phase via siloxane linkage (details on the coupling reaction can be found in ref. 23).

Solid shells. Positively charged polystyrene particles of about 600 nm in diameter are prepared by surfactant-free emulsion polymerization using 2,2′-azobis (2-methylpropionamidine) dihydrochloride (97% from Sigma-Aldrich) as radical initiator. 50 ml of styrene monomer (≥99% from Sigma-Aldrich) is passed through an activated aluminium oxide column to remove inhibitor, and then added to a 1-l three-neck round bottom flask containing 500 ml of deionized water. The mixture is set under nitrogen atmosphere and emulsified by a mechanical stirrer operating at 330 r.p.m. After 30 min the temperature is raised to 60 °C and the polymerization started by adding 0.5 g of initiator. After 16 h the mixture is brought to room temperature and the particles set in deionized water via three cycles of centrifugation and re-suspension. Larger particles (>600 nm) are obtained by repeated seeded growth (Extended Data Fig. 1e–h). PVP-stabilized (average molecular weight 10,000 g mol^{-1}, Sigma-Aldrich) polystyrene particles are prepared by dispersion polymerization following the procedure in ref. 24. In brief, 50 g styrene are added to 400 g ethanol followed by addition of 5 g PVP and 1 g 2,2′-azobisisobutyronitrile (98%, Sigma-Aldrich). The mixture is then brought to 65 °C and stirred at 330 r.p.m. for 16 h. Particles of approximately 2.6 μm are purified and transferred in deionized water via three sequential washes, in ethanol, ethanol/deionized water mixture and deionized water.

Assembly of LCCs. Clusters are prepared from binary mixtures of PS particles and silicone oil droplets via a relatively simple heteroaggregation process (Extended Data Fig. 2a). Their successful assembly, however, requires the careful adjustment of four key parameters:

(i) The size ratio α between the PS spheres and the emulsion droplets determines the coordination number of the population of the main cluster, and its optimal value is chosen on the basis of computer simulations[16]. In our experiments, we used $\alpha = 3.00$, $\alpha = 1.98$ and $\alpha = 1.31$ to assemble trimers, tetramers and hexamers, respectively.

(ii) The second parameter is the attractive driving force between PS spheres and the emulsion droplets. In our experiments, we used electrostatic attractions between positively charged PS spheres and negatively charged oil droplets, and polymer bridging flocculation between PVP-coated PS spheres and oil droplets. To promote polymer-bridging flocculation, the suspensions were mixed in the presence of 25 mM NaCl.

(iii) The number density ratio η between PS spheres and the emulsion droplets was taken to be $\eta \geq 100$ to prevent the formation of bridged particle aggregates. A high shell concentration also favours a rapid parking of PS spheres around the droplets, allowing the cluster to reach maximum coordination before wetting forces can cause any substantial geometrical distortion to partially coordinated intermediates.

(iv) The fourth parameter is the wetting angle θ between the oil and the PS surface. In simulations, α is determined for hard spheres that stick irreversibly and randomly to each other; however, in our system, the spheres can effectively interpenetrate each other owing to the liquid nature of the core particles. To better approximate the interactions between hard spheres, we maximize the wetting angle θ during the initial coordination step. For LCCs assembled from oppositely charged building blocks, this is typically achieved by re-suspending the emulsion droplets and the PS spheres in 25 mM HCl aqueous solution before their mixing. The coordination is then carried out by dripping 5 ml of emulsion (0.04 wt%) into 5 ml of a PS suspension (4 wt%) at a rate of 1 ml min^{-1} under mild stirring. LCCs prepared by polymer bridging flocculation were mixed in a similar manner. In this case, however, PVP–PS suspensions and emulsion are re-suspended in 25 mM NaCl instead of acid.

After their assembly, LCCs are isolated from the excess singlets by exploiting the density mismatch between the PS spheres (1.05 g cm^{-3}) and the oil droplets (1.23 g cm^{-3} for methacrylate-functionalized droplets). The mixture is suspended in an approximately 22 wt% glycerol/water solution and centrifuged at 3,500*g* for 1 h, during which the light singlets rise to the top of the vial and the heavier LCCs sediment at the bottom. Typically, the exact glycerol concentration is empirically tuned to yield a clear split of the two species. Notably, the coordination and separation techniques are not size-dependent. As long as the size ratio and number ratio of the two species are kept constant, nanometre-sized tetrahedral clusters are fabricated and purified from PS singlets in the same manner as for their micrometre-sized counterparts (Extended Data Fig. 2b,c).

Statistical distributions of the clusters were measured by optical video microscopy. LCC suspensions were studied in 50-mm-long glass capillary tubes (inner dimensions 2.0 mm × 0.1 mm, VitroCom) mounted on the stage of an inverted optical microscope. Microscopy videos were acquired using a 100× oil immersion objective while scanning throughout the length of the capillary. The videos were then played back to identify and count all clusters in the field of view. Typically ≥200 particles were counted for each sample. Figure 1f–h shows the large field of view of the raw (not purified) suspensions used for the statistical analysis.

Colloidal fusion. Colloidal fusion is initiated by introducing a water-soluble plasticizer (THF) to a LCC suspension. The process is sensitive to THF concentration and the type of polystyrene used. For clusters assembled from PVP-stabilized PS, the THF concentration necessary for an optimal colloidal fusion is between 20% and 35%. Within this range the deformation of LCCs into patchy particles occurs in a consistent and reproducible manner. Lower THF concentrations are generally not sufficient to deform the clusters, whereas exposure to THF concentrations above 40% result in less homogeneous patchy patterns. To minimize the effect of THF gradients during mixing and obtain a uniform fusion process, we typically add a freshly prepared 40% v/v THF/water mixture to the LCC suspension in a 1:1 volume ratio. All of the deformations are allowed to proceed for 20 s before quenching the system in deionized water. Fusion of positively charged PS spheres generally requires slightly higher THF concentrations compared to PVP-stabilized PS spheres. For example, for the same deformation time of 20 s, a minimum THF concentration of 30% (instead of 20%) is necessary. The process of colloidal fusion may be applied to many other liquids. However, there are some basic requirements that need to be considered. (i) The assembly of LCCs relies on precise core-to-shell size ratios, and it is therefore crucial to utilize monodispersed building blocks. We met this requirement by chemically synthesizing oil droplets via nucleation and growth process. Although this is rather simple to realize with alkoxysilanes, different oil phases may require different emulsification methodologies. (ii) The assembly of LCCs requires an attractive interaction between core and shell building blocks. Two of the simplest binding mechanisms are electrostatic forces and polymer-mediated interactions. This requires oil droplets with charged or polymer-coated interfaces. (iii) To preserve the LCC symmetry, the oil and plasticized shells should not mix. (iv) To favour the extrusion of the core, the interfacial tension $\gamma_{PSl/o}$ between the oil and the plasticized shell material should be lower than $\gamma_{o/w}$ and $\gamma_{PSl/w}$.

Liquid patches were occasionally hardened to allow for SEM analysis. Depending on the chemistry of the oil precursor used in the preparation of the droplets, different hardening methods were used. Methacrylate-functionalized patches were polymerized at 80 °C by using KPS (5 mM) or AIBN (20 mg) as radical initiators. Chlorinated patches were hardened by promoting cross-linking in 100 mM NH_3 solution overnight. Solid epoxy-functionalized patches were obtained by radical polymerization of hybrid droplets containing both (3-glycidyloxypropyl) trimethoxy silane and 3-(trimethoxysilyl)propyl methacrylate in a 50:50 volume ratio.

If the fusion of LCCs takes place at pH 2, faceted tetrahedral cores can be captured as an intermediate. Typically, THF solution (40% in water) is added to the LCC suspension to a final concentration of 21%. After 10 min, 25 mM HCl solution is dripped to the deformed clusters to reach an eightfold dilution. To recover the new colloidal shape, the core is first hardened by polymerization and then the PS matrix is dissolved in pure THF.

Variation of oil–PS wetting angle. The large difference between the isoelectric points of oil (pH of about 6) and PS (pH of about 10) enables us to tune the wetting angle θ between the two materials by simply changing the pH of the suspension. At pH 2, oil and PS are both positively charged, which results in a fairly large wetting angle (red zone in Extended Data Fig. 3a). As the pH approaches 7, however, the oil undergoes a charge inversion causing the now oppositely charged surfaces to attract each other (green zone in Extended Data Fig. 3a). As we show in Extended Data Fig. 3b, this electrostatic attraction manifests as a marked decrease in the value of θ.

These wetting conditions have important effects in the assembly of LCCs. For example, as we show in Extended Data Fig. 3c, d, the core of an LCC deforms and spreads visibly more at pH 7 than at pH 2.

Surface tension measurements. Interfacial tensions are measured using the pendant drop method (Attension Theta Optical Tensiometer, Biolin Scientific). Macroscopic oil phases are collected by forced coalescence of freshly prepared emulsions. This is typically realized by bringing the droplets to their isoelectric point with the addition of 25 mM HCl, and then sedimenting them by centrifugation at 3,500*g* for 30 min. The resulting viscous oil phase is then isolated and equilibrated against the desired aqueous phase before each measurement.

To obtain a liquid PS phase, PS particles are suspended in 60% THF and centrifuged at 3,500*g* for 30 min. Here we note that although colloidal fusion is performed at lower THF concentrations (20% THF for PVP–PS; 40% THF for positively charged PS), 60% THF is necessary to obtain a macroscopic PS phase that is sufficiently fluid to be handled by the tensiometer.

Computer simulations. We use the Surface Evolver package[21,22] to simulate the structural evolution of LCCs to patchy particles. An initial surface, defined in a script file, is evolved towards minimal energy using a gradient-descent method. The surface is implemented as a simplicial complex in which each cell can be progressively refined by a triangular tessellation to achieve the desired level of accuracy. On each iteration step, Surface Evolver minimizes the energy by changing surface along the negative gradient direction of surface energy until it reaches a local minimum.

To simulate colloidal fusion we consider an LCC composed of liquefied PS particles assembled on a central silicone oil droplet. The interfacial tensions between the constituents materials of the cluster are indicated as $\gamma_{PSl/w}$, $\gamma_{o/w}$ and $\gamma_{PSl/o}$, where 'w' indicates the aqueous plasticizing solution (20%–40% THF), PSl the liquefied polystyrene and 'o' the silicone oil. In Extended Data Fig. 5 these values refer to the green, yellow and red surfaces, respectively.

A typical simulation is set up as follows: (i) $\gamma_{PSl/w}$ is set to 50 mN m^{-1} and $\gamma_{o/w}$ to 36 mN m^{-1} to match the measured experimental values; (ii) the oil-to-PS volume ratio (V_o/V_{PS}) is kept constant during the evolution, and its value is chosen according to the experimental geometry (for example, 0.125 for a tetrahedral LCC and 0.5 for an octahedral LCC); and (iii) we allow the PS particles to deform but not to coalesce (PS–PS surfaces do not disappear), and set $\gamma_{PSl/PSl} \leq 0.01$ mN m^{-1}.

In the first set of simulations (Extended Data Fig. 5a), we looked at the effect of $\gamma_{PSl/o}$ on the evolution of a tetrahedral LCC. For $\gamma_{PSl/o} \geq 10$ mN m^{-1}, the liquid core fails to extrude trough the interstices of the cluster and instead retracts, forming a spherical core. However, as $\gamma_{PSl/o}$ decreases below 10 mN m^{-1}, the liquid core reaches the surface of the particle, forming four oil–water interfacial patches that progressively increase in size as $\gamma_{PSl/o}$ decreases (yellow areas in Extended Data Fig. 5a).

As shown above, we can change $\gamma_{PSl/o}$ experimentally by tuning the surface charge of oil and PS. At pH 2, for example, oil and PS surfaces are both positively charged, resulting in a relatively high value of $\gamma_{PSl/o}$. At these conditions, LCCs evolve to core–shell particles as predicted by the simulations. However, as the pH reaches 7, the oil surface undergoes a charge-inversion, lowering $\gamma_{PSl/o}$ and prompting patch formation.

Simulations with $\gamma_{PSl/o} = 5$ mN m^{-1} yield patchy morphologies that are very close to those observed in the experiments. A nearly perfect match, however, results from simulations in which we evolve the LCCs in two steps (Extended Data Fig. 5b). In the first step, the cluster is allowed to evolve at $\gamma_{PSl/o} = 3$ mN m^{-1}, which results in the complete extrusion on the liquid core onto the surface of the particle. This intermediate state is then further evolved at higher values of $\gamma_{PSl/o}$. In this second evolution, the patches, which were initially widely spread onto the surface of the particle, compact into lentil-like shapes that closely resemble the experimental morphologies. We can rationalize this tuning step as the result of slight changes in the experimental conditions (such as THF evaporation or oil ageing) that occur after the initial fusion and cause small changes in $\gamma_{PSl/o}$. We explored the simulation parameter space further by investigating the effect of V_o/V_{PS} on the fusion process. These simulations, summarized in the phase diagram in Extended Data Fig. 5c, show that the ratio V_o/V_{PS} could also be used to tune the evolution of LCCs in experiments.

Colloidal fusion is not limited to tetrahedral clusters; in Extended Data Fig. 6, we demonstrate that Surface Evolver simulations also correctly predict the formation of eight-patch particles from octahedral LCCs ($N = 6$). The simulated fusion of an LCC into a patchy particle also reveals the internal microstructure of the particle throughout the intermediate stages of its transformation. Because these transient structures can be observed experimentally using fluorescent liquid cores and fixed by polymerization, Surface Evolver simulations can be used as a computer-aided design tool for the fabrication of new colloidal geometries. This is exemplified in Extended Data Fig. 4, in which we show the evolution of a tetrahedral LCC for $\gamma_{PSl/o} = 40$ mN m^{-1}. As expected for such a high value of $\gamma_{PSl/o}$, the cluster transforms into a spherical core–shell particle. However, during the transformation the core undergoes a series of morphological changes that include the formation of a regular tetrahedron. This intermediate microstructure was experimentally isolated in the laboratory and used to fabricate the colloidal tetrahedra shown in the SEM image in Extended Data Fig. 4.

Liquid bonding. To demonstrate directional bonding between patches and target particles, we use patchy particles with charge-stabilized patches and a polymer-stabilized body. When the ionic strength of the suspension is raised to 25 mM NaCl, charge screening effects make the patches sticky and keen to bind to neighbouring particles. The supracolloidal structures shown in Extended Data Fig. 7, for example, are assembled by dripping a dilute patchy particle suspension (<0.5 wt% in 25 mM NaCl aqueous solution) into a concentrated suspension of PVP-stabilized PS spheres (about 5 wt% in 25 mM NaCl aqueous solution). After the assembly, the decorated patchy particles are isolated by filtration through a 5-μm-pore membrane. To enable SEM analysis, the liquid bridges are permanently fixed via a radical polymerization. Patch-to-patch liquid bonds are formed by adding HCl to patchy particle suspensions to a final concentration of 25 mM. The acid increases the ionic strength of the system and quenches the negative charges at the oil–water interface, thus causing coalescence between adjacent patches and the formation of liquid bridges. To facilitate the formation of patch- to-patch bonds, liquid patches are pre-swollen using Pluronic L61 (Extended Data Fig. 8). Typically, 1 μl of Pluronic L61 is added to 100 μl of patchy particle suspension (0.5 wt%) and mixed for a few seconds using a vortex mixer. Selective swelling is achieved within a few minutes without compromising the stability of the colloidal system. The swollen patchy particles are then suspended in 25 mM HCl to promote coalescence between adjacent patches and the formation of liquid bonds. Optimal bonding is achieved by pre-swelling the patches to two to three times their original volume. The degree of swelling, which ultimately depends on the ratio of Pluronic L61 to silicon oil in the system, can be empirically tuned by adding Pluronic L61 in small aliquots and using optical microscopy as feedback. In our experiments, we were able to swell patches up to ten times their initial volume. In their swollen state the patches cannot be polymerized directly, because they are composed mainly of Pluronic L61surfactant. De-swelling, however, can be achieved by dialysis or dilution.

Curvature of the patches. Owing to their liquid nature, the patches can change their morphology from convex, to flat, to concave. The easiest way to alter their morphology is to gradually reduce their volume by degrading the oil in 50 mM NaOH. The basic environment causes the constituent silsesquioxanes of the oil to hydrolyze, and the patches to shrink. The etching process can be stopped at an intermediate stage by quenching the mixture with deionized water, or allowed to proceed to completion, which would result in concave patches. Alternatively, the complete dissolution of the patches can be achieved by washing the particles in ethanol, which is a good solvent for the oil.

Finally, we note that we have consistently observed flat patches forming when a different nucleation protocol was used for the preparation of the silicone oil droplets. In the modified protocol, the oil precursor is allowed to pre-hydrolyse in deionized water instead of being added to the nucleating ammonia solution directly. Ongoing research is trying to elucidate the cause of this different behaviour.

EDS analysis. Energy-dispersive X-ray spectroscopy (EDS, Oxford Instruments) is used to characterize the chemical contrast between the patches and matrix of a particle. Figure 3c shows a typical EDS analysis in which a line scan reveals the relative elemental abundance across the surface of a patchy particle. As expected, the elements that characterize the silane precursor (here (3-chloropropyl) trimethoxy silane) are found only on the patch area, confirming the chemical anisotropy of the surface of the particle.

Data availability. The data that support the findings of this study are available from the corresponding author on request.

23. Sacanna, S., Rossi, L., Kuipers, B. & Philipse, A. Fluorescent monodisperse silica ellipsoids for optical rotational diffusion studies. *Langmuir* **22,** 1822–1827 (2006).
24. Lee, J., Ha, J. U., Choe, S., Lee, C.-S. & Shim, S. E. Synthesis of highly monodisperse polystyrene microspheres via dispersion polymerization using an amphoteric initiator. *J. Colloid Interface Sci.* **298,** 663–671 (2006).

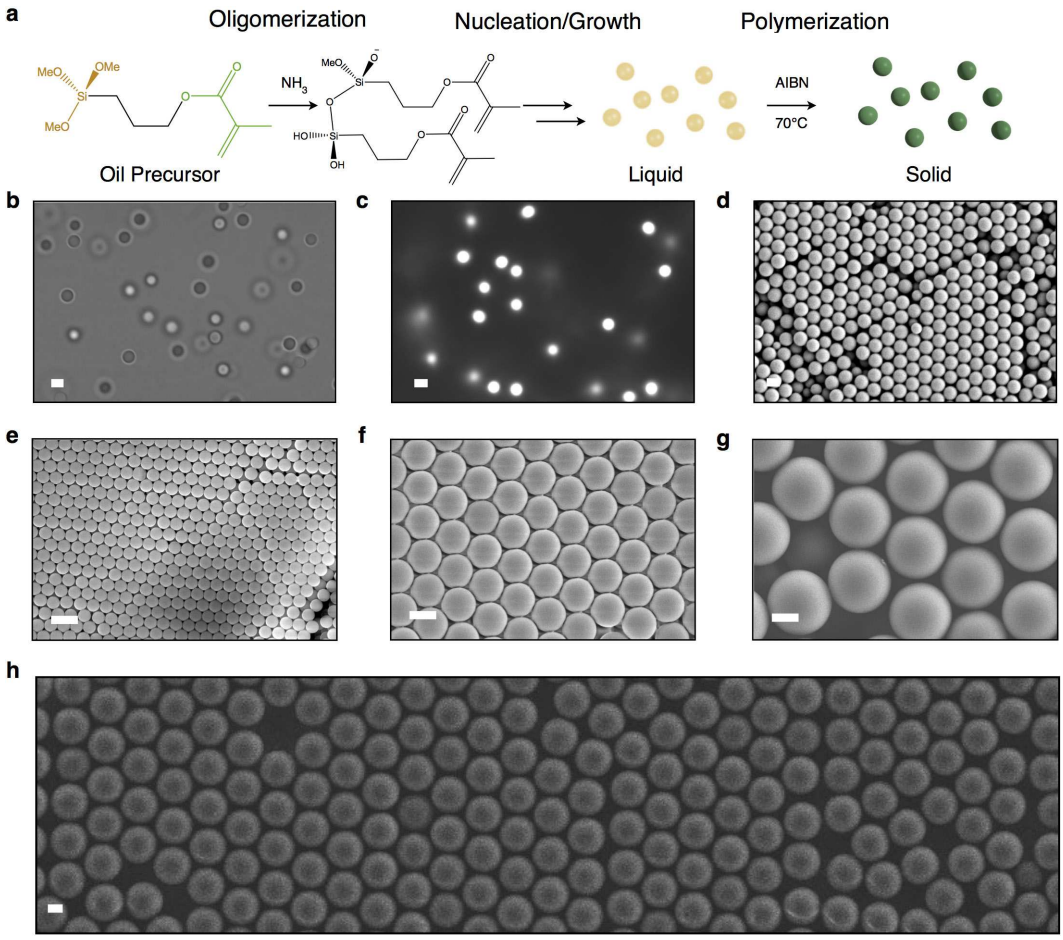

Extended Data Figure 1 | Synthesis of the constituent building blocks of the LCCs. a, Schematic representation of the spontaneous emulsification and subsequent polymerization of 3-(trimethoxysilyl)propyl methacrylate. **b**, Bright-field microscopy image showing monodispersed emulsion droplets prepared from 3-(trimethoxysilyl)propyl methacrylate oil precursor. **c**, Fluorescence microscopy image showing emulsion droplets labelled with rhodamine B. **d**, SEM image of a polymerized emulsion. **e**–**g**, SEM images documenting the growth of positively charged PS particles during the three steps of seeded emulsion polymerization. **h**, PVP–PS particles prepared by dispersion polymerization. Scale bars are 1 μm.

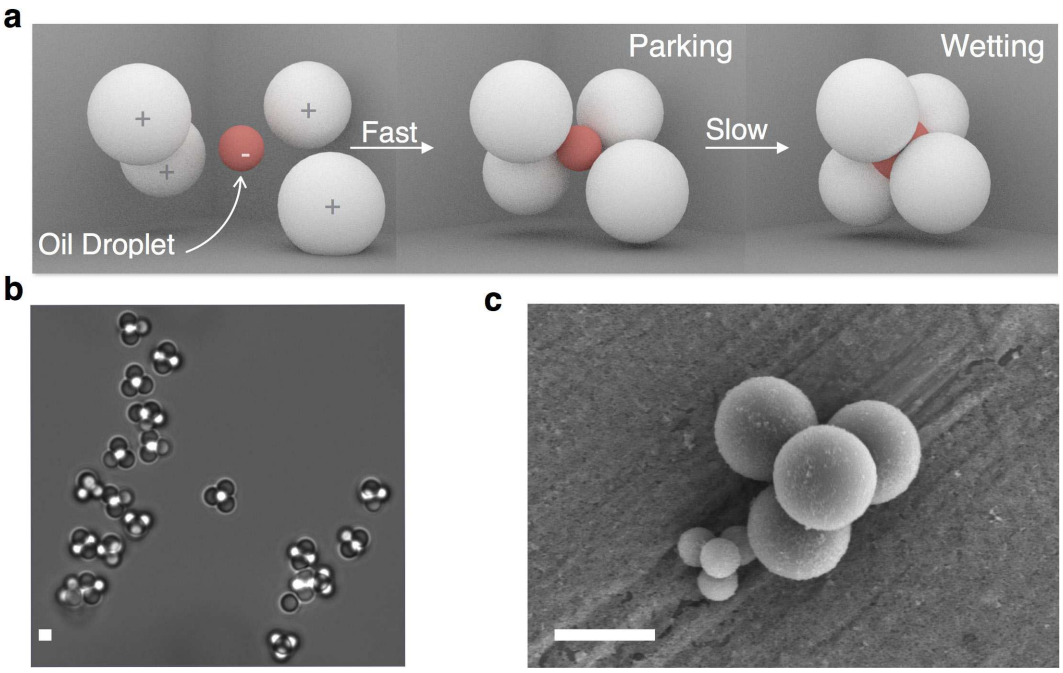

Extended Data Figure 2 | Self-assembly on a LCC. a, Schematics showing the assembly of an LCC via electrostatic attraction. Rapid parking of PS spheres on droplets followed by slower wetting dynamics ensures high yields of regular tetrahedral clusters. **b**, Bright-field microscopy image showing tetrahedral LCCs isolated by density splitting. **c**, SEM image showing a micrometre-sized cluster next to a nanometre-sized cluster. Scale bars are 1 μm.

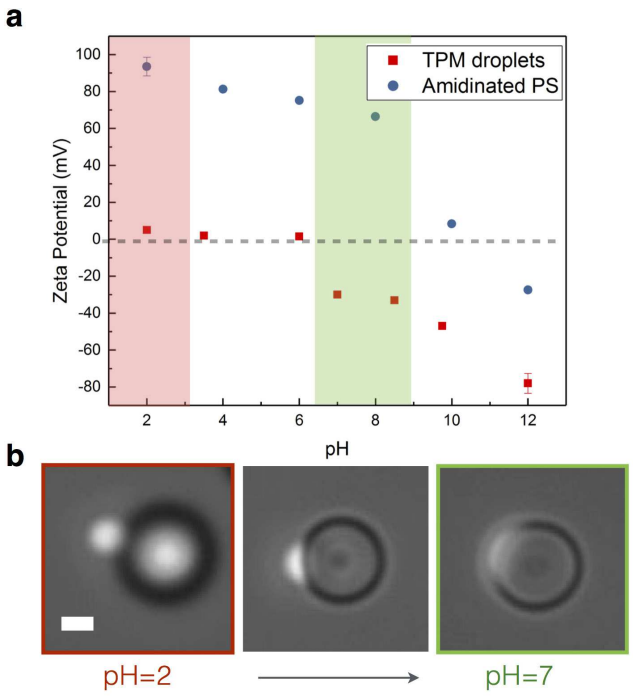

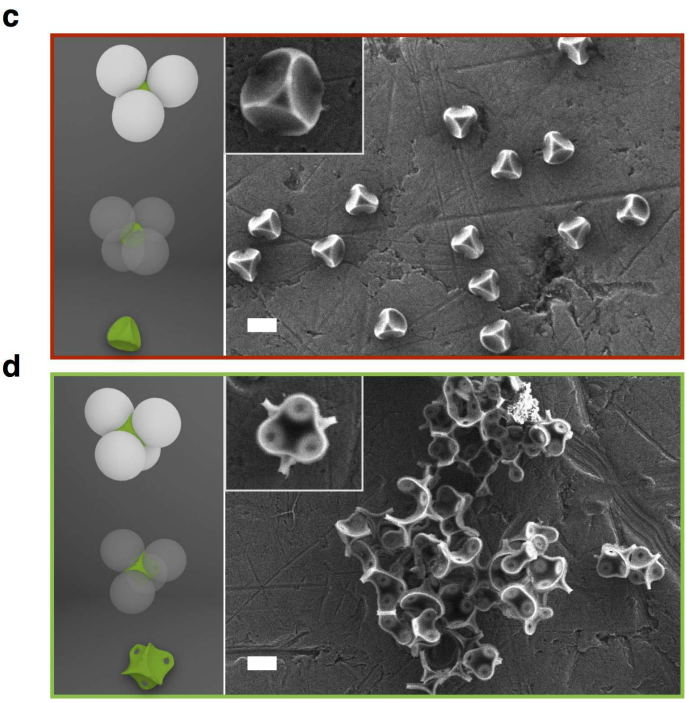

Extended Data Figure 3 | Tuning of the oil–PS contact angle. a, Zeta potential of oil droplets (3-(trimethoxysilyl)propyl methacrylate, TPM) and amidinated PS particles as a function of pH (Malvern Zetasizer Nano Series). **b**, Wetting behaviour of a fluorescent oil droplet on an amidinated PS sphere at different pH. **c**, **d**, Left, schematics of the recovery of solid cores (green) from LCCs. Right, SEM images of recovered cores (polymerized), imprinted by PS shells at low (**c**) and neutral (**d**) pH. Scale bars are 1 μm.

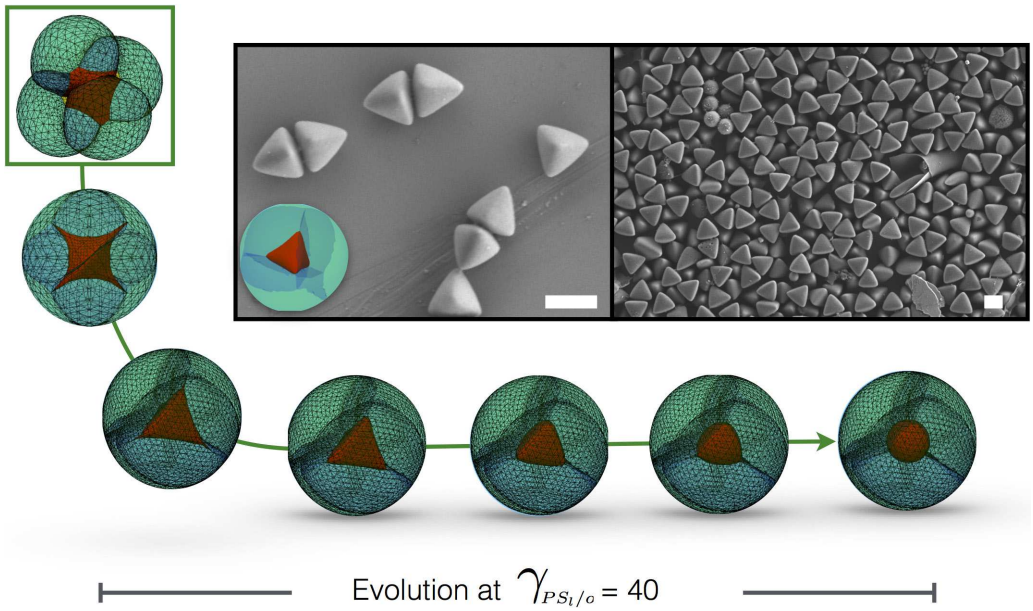

Extended Data Figure 4 | Design and realization of faceted tetrahedra. Simulated fusion of a tetrahedral LCC into a spherical core–shell particle is shown for $\gamma_{PSl/o} = 40$ mN m^{-1}. The snapshot sequence reveals the morphological transformation of the liquid core (red) in great detail. During the intermediate stages of the transformation, the core is gradually reshaped into a faceted tetrahedron. This intermediate deformation stage can be targeted experimentally to fabricate the colloidal tetrahedra shown in the SEM images. Scale bar is 1 μm.

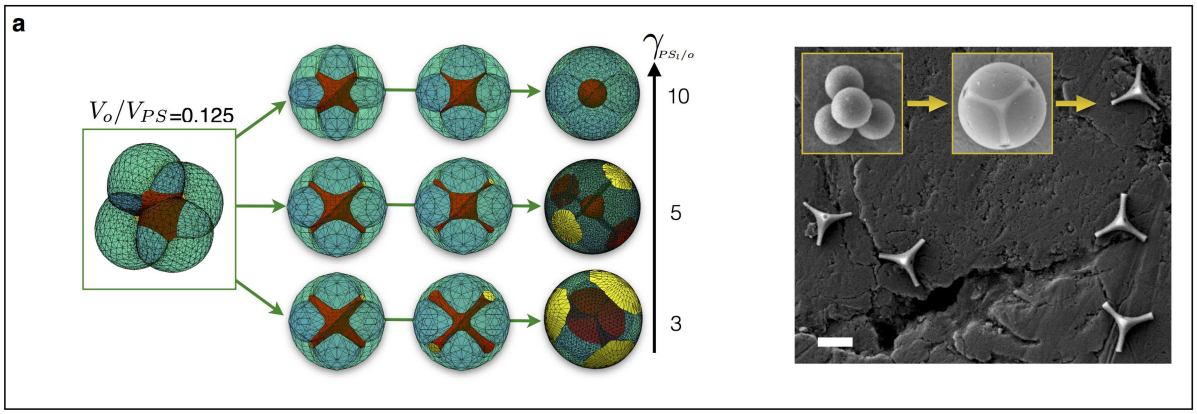

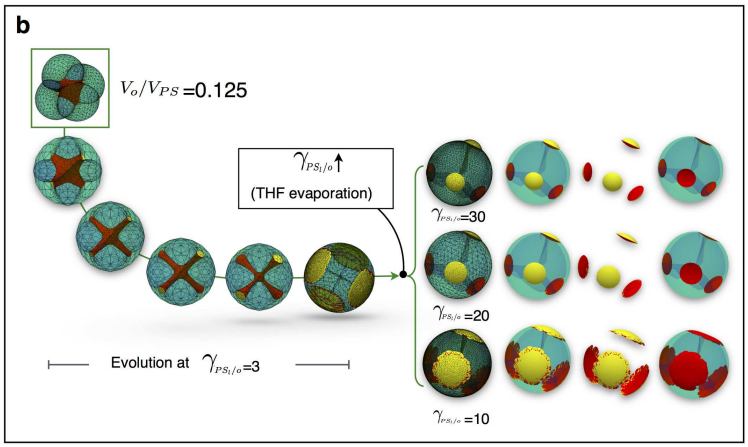

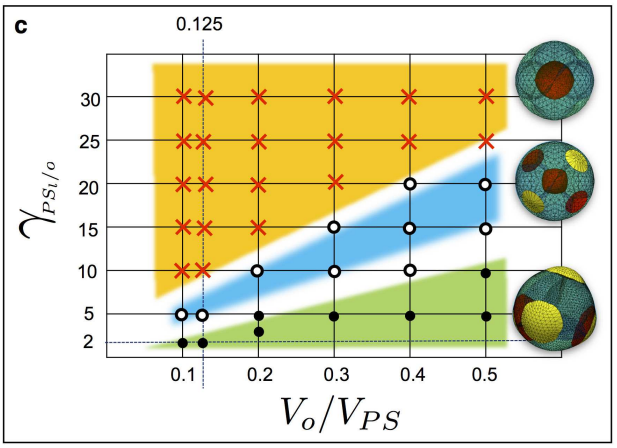

Extended Data Figure 5 | Simulated fusion of tetrahedral LCCs. **a**, Surface Evolver simulations probing the effect of $\gamma_{PSl/o}$ (red surface) on the evolution pathway of the cluster. The values of $\gamma_{PSl/w} = 50$ mN m^{-1} (green surface), $\gamma_{o/w} = 36$ mN m^{-1} (yellow surface) and $V_o/V_{PS} = 0.125$ are chosen to match the corresponding experimental values. We can follow the morphological evolution of the liquid cores experimentally by fixing intermediate states by radical polymerization. The hardened cores are isolated by dissolving the PS matrix and analysed using SEM (right). Scale bar is 1 μm. **b**, A comparison between simulations and experiments suggest a two-step evolution process in which $\gamma_{PSl/o}$ increases during the deformation. Experimentally, this could be rationalized by considering the change in the THF concentration during the evaporation process or the ageing of the oil phase. **c**, Phase diagram showing how $\gamma_{PSl/o}$ and V_o/V_{PS} can predictably change the evolutionary fate of a tetrahedral LCC undergoing colloidal fusion.

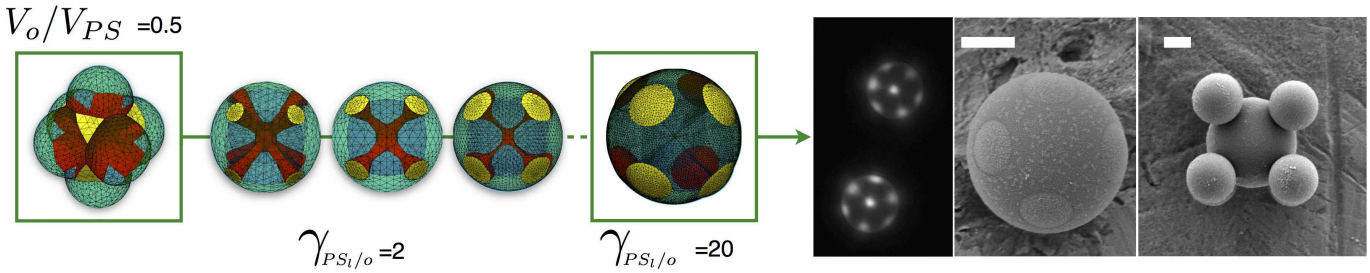

Extended Data Figure 6 | Simulated fusion of octahedral LCCs. The simulated evolution proceeds in two consecutive steps (see also Extended Data Fig. 5b). The first step, with $\gamma_{PSl/o} = 2\ mN\ m^{-1}$, correctly evolves the cluster into an eight-patch particle; the second step, with $\gamma_{PSl/o} = 20\ mN\ m^{-1}$, further refines the patch morphology to a nearly perfect match with the experimental results. On the right is a fluorescence microscopy image of eight-patch particles and SEM images showing the patchy particle before and after coordination with PS singlets. Scale bars are 1 μm.

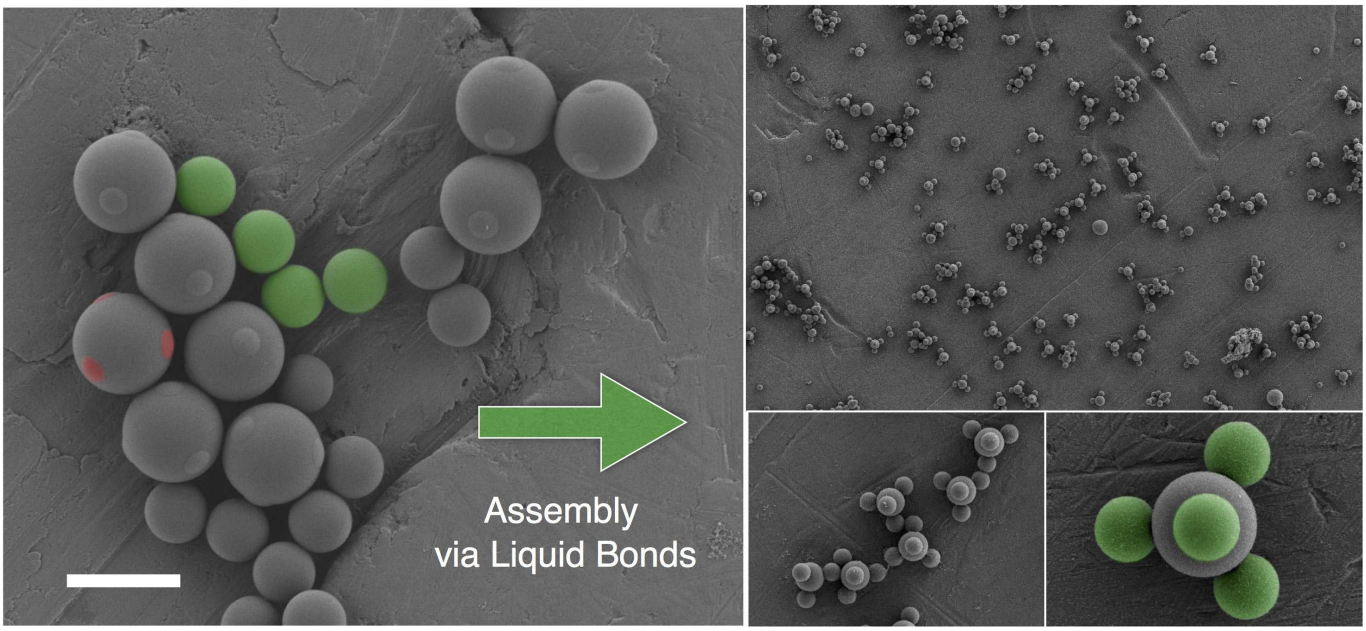

Extended Data Figure 7 | Supracolloidal assembly via liquid bonds. False-colour SEM images of patchy particles (red) mixed with PVP–PS singlets (green). The images (at increasing magnification) show supracolloidal architectures assembled via liquid bonds. Scale bar is 5 μm.

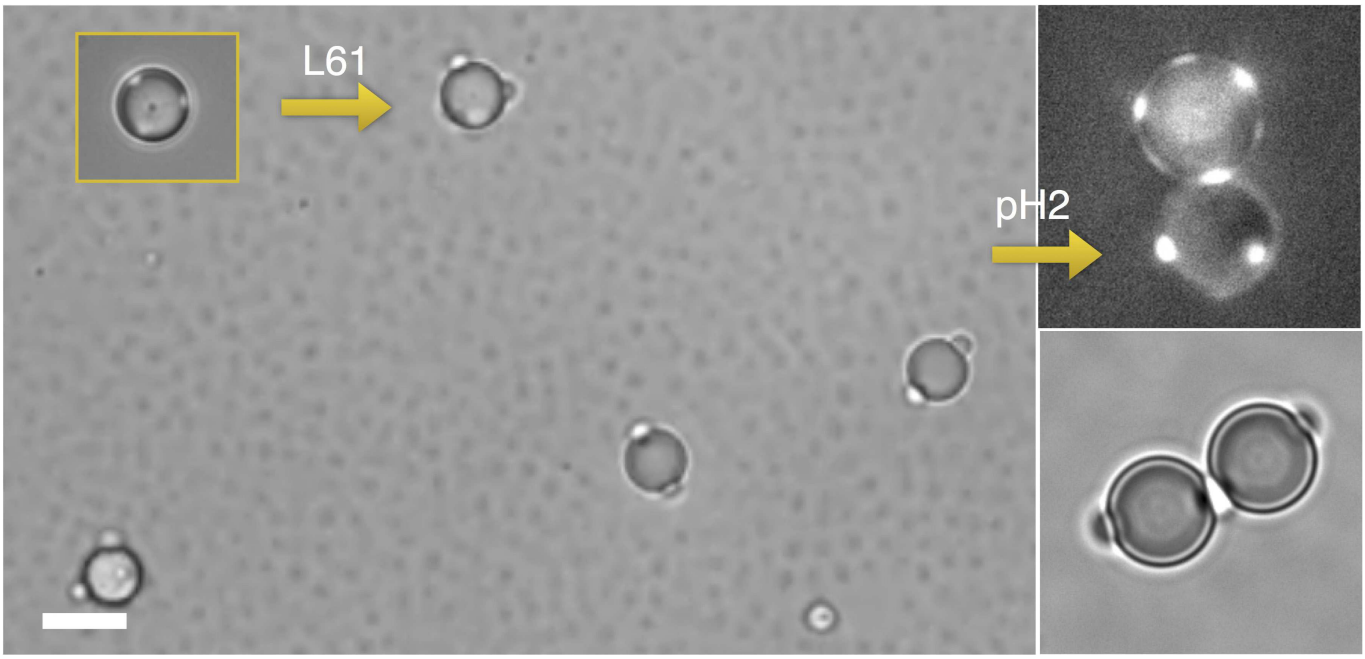

Extended Data Figure 8 | Patch-swelling and formation of patch-to-patch liquid bridges. Bright-field and fluorescence microscopy images are shown. The patchy particles are first exposed to Pluronic L61, which selectively swells the patches, which tend to coalesce and thus form liquid bonds under acidic conditions. Scale bar is 5 μm.